its linear value of 0.42 to a value of 0.27 ± 0.015 at this intensity. Both the real and the imaginary parts of the refractive index saturate for even higher input power. We found that these measurements are highly repeatable and that the material does not exhibit a permanent change of its optical properties.

The magnitude of the optically induced ultrafast change of the real part of the refractive index (Δn = 0.72 ± 0.025) and the relative change of 170% in comparison to the linear value are unprecedented. The change in the refractive index corresponds to a change of the permittivity from $\varepsilon = 0 + 0.352i$ to $\varepsilon = 1.22 + 0.61i$ where i is the square root of −1. This result shows that ITO can exhibit a reversible transition from metallic to a lossy dielectric state with a subpicosecond time response at wavelengths slightly longer than the bulk plasmon wavelength. Moreover, the usual perturbation expansion description of nonlinear optical effects is not applicable for this material at high intensities.

We have shown that a thin ITO film exhibits an extremely large ultrafast third-order nonlinearity at ENZ wavelengths. Moreover, it can acquire an optically induced change in the refractive index that is unprecedentedly large. Our results challenge the notion that the nonlinear optical response is only a perturbation to the linear response. Materials with such a large nonlinear response are expected to enable exotic nonlinear dynamics (*22*) and allow all-optical control of metasurface and active plasmonics devices. Thus, our results introduce a completely new paradigm in nonlinear optics and open new avenues for developing optical nanostructures with large nonlinearity for applications in nanophotonics, plasmonics, and nonlinear nano-optics.

REFERENCES AND NOTES

1. M. Kauranen, A. V. Zayats, *Nat. Photonics* **6**, 737–748 (2012).
2. M. Abb, P. Albella, J. Aizpurua, O. L. Muskens, *Nano Lett.* **11**, 2457–2463 (2011).
3. M. Silveirinha, N. Engheta, *Phys. Rev. Lett.* **97**, 157403 (2006).
4. A. Alù, M. Silveirinha, A. Salandrino, N. Engheta, *Phys. Rev. B* **75**, 155410 (2007).
5. A. R. Davoyan, A. M. Mahmoud, N. Engheta, *Opt. Express* **21**, 3279–3286 (2013).
6. A. D. Neira *et al.*, *Nat. Commun.* **6**, 7757 (2015).
7. H. Suchowski *et al.*, *Science* **342**, 1223–1226 (2013).
8. A. Capretti, Y. Wang, N. Engheta, L. Dal Negro, *Opt. Lett.* **40**, 1500–1503 (2015).
9. T. S. Luk *et al.*, *Appl. Phys. Lett.* **106**, 151103 (2015).
10. N. Kinsey *et al.*, *Optica* **2**, 616 (2015).
11. G. V. Naik, V. M. Shalaev, A. Boltasseva, *Adv. Mater.* **25**, 3264–3294 (2013).
12. E. Feigenbaum, K. Diest, H. A. Atwater, *Nano Lett.* **10**, 2111–2116 (2010).
13. M. Sheik-Bahae, A. A. Said, T.-H. Wei, D. J. Hagan, E. W. Van Stryland, *IEEE J. Quantum Electron.* **26**, 760–769 (1990).
14. B. K. Rhee, J. S. Byun, E. W. Van Stryland, *J. Opt. Soc. Am. B* **13**, 2720 (1996).
15. H. I. Elim, W. Ji, F. Zhu, *Appl. Phys. B* **82**, 439–442 (2006).
16. See supplementary materials on *Science* Online.
17. R. W. Boyd, *Nonlinear Optics* (Elsevier, 2008).
18. C. Sun, F. Vallée, L. Acioli, E. P. Ippen, J. G. Fujimoto, *Phys. Rev. B Condens. Matter* **48**, 12365–12368 (1993).
19. S. D. Brorson, J. G. Fujimoto, E. P. Ippen, *Phys. Rev. Lett.* **59**, 1962–1965 (1987).
20. E. Carpene, *Phys. Rev. B* **74**, 024301 (2006).
21. B. Rethfeld, A. Kaiser, M. Vicanek, G. Simon, *Phys. Rev. B* **65**, 214303 (2002).
22. D. de Ceglia, S. Campione, M. A. Vincenti, F. Capolino, M. Scalora, *Phys. Rev. B* **87**, 155140 (2013).

ACKNOWLEDGMENTS

The authors gratefully acknowledge the support of the Canada Excellence Research Chairs Program. R.W.B. is the cofounder and Chief Technology Officer of KBN Optics, Pittsford, NY.

SUPPLEMENTARY MATERIALS

www.sciencemag.org/content/352/6287/795/suppl/DC1
Materials and Methods
Supplementary Text
Figs. S1 to S4
References (*23*–*32*)

7 December 2015; accepted 12 April 2016
Published online 28 April 2016
10.1126/science.aae0330

CATALYSIS

Photochemical route for synthesizing atomically dispersed palladium catalysts

Pengxin Liu,[1] Yun Zhao,[1] Ruixuan Qin,[1] Shiguang Mo,[1] Guangxu Chen,[1] Lin Gu,[2] Daniel M. Chevrier,[3] Peng Zhang,[3] Qing Guo,[1] Dandan Zang,[1] Binghui Wu,[1] Gang Fu,[1]* Nanfeng Zheng[1]*

Atomically dispersed noble metal catalysts often exhibit high catalytic performances, but the metal loading density must be kept low (usually below 0.5%) to avoid the formation of metal nanoparticles through sintering. We report a photochemical strategy to fabricate a stable atomically dispersed palladium–titanium oxide catalyst (Pd_1/TiO_2) on ethylene glycolate (EG)–stabilized ultrathin TiO_2 nanosheets containing Pd up to 1.5%. The Pd_1/TiO_2 catalyst exhibited high catalytic activity in hydrogenation of C=C bonds, exceeding that of surface Pd atoms on commercial Pd catalysts by a factor of 9. No decay in the activity was observed for 20 cycles. More important, the Pd_1/TiO_2-EG system could activate H_2 in a heterolytic pathway, leading to a catalytic enhancement in hydrogenation of aldehydes by a factor of more than 55.

Atomically dispersed catalysts with mononuclear metal complexes or single metal atoms anchored on supports have recently attracted increasing research attention (*1*–*15*). With 100% metal dispersity, atomically dispersed catalysts offer the maximum atom efficiency, providing the most ideal strategy to create cost-effective catalysts, particularly those based on Earth-scarce metals such as Pt (*1*–*5*), Au (*5*–*8*), Pd (*9*–*12*), and Ir (*13*, *14*). Moreover, the uniform active sites of atomically dispersed catalysts make them a model system to understand heterogeneous catalysis at the molecular level (*4*, *6*, *10*, *12*–*14*, *16*–*21*), bridging the gap between heterogeneous and homogeneous catalysis.

During the past decade, several strategies for atomically dispersing metal sites on catalyst supports have emerged; these include lowering the loading amount of metal components (*1*, *8*–*10*, *12*, *20*), enhancing the metal-support interactions (*4*, *6*, *9*, *19*), and using voids in supports or vacancy defects on supports (*3*, *11*, *14*, *22*). In most cases, the supports for atomically dispersed catalysts are deliberately chosen. Zeolites provide effective voids to anchor individual metal atoms therein and prevent them from sintering during catalysis (*23*, *24*). Defects on reducible oxides (e.g., TiO_2 and CeO_2) (*25*, *26*) and on graphene or C_3N_4 (*9*, *11*, *22*) help to stabilize atomically dispersed metal atoms on supports. Coordinatively unsaturated Al^{3+} ions on γ-Al_2O_3 act as binding centers to maintain the high dispersion of Pt atoms, but Pt rafts form as the loading amount of Pt increases (*3*). Currently, two major challenges remain in the field of atomically dispersed catalysts: (i) to ensure a loading content high enough for practical applications while maintaining the metal centers as individual sites under catalytic conditions (*27*, *28*), and (ii) to address whether atomically dispersed catalysts offer distinct active sites and/or undergo catalytic pathways different from those of conventional metal catalysts (*1*, *4*–*6*, *8*–*10*, *12*, *16*–*21*).

We report a room-temperature photochemical strategy to fabricate a highly stable, atomically dispersed Pd catalyst (Pd_1/TiO_2) on ultrathin TiO_2 nanosheets with Pd loading up to 1.5%.

[1]State Key Laboratory for Physical Chemistry of Solid Surfaces, Collaborative Innovation Center of Chemistry for Energy Materials, Engineering Research Center for Nanopreparation Technology of Fujian Province, National Engineering Laboratory for Green Chemical Productions of Alcohols, Ethers, and Esters, and Department of Chemistry, College of Chemistry and Chemical Engineering, Xiamen University, Xiamen 361005, China. [2]Institute of Physics, Chinese Academy of Sciences, Beijing 100190, China. [3]Department of Chemistry, Dalhousie University, Halifax, Nova Scotia B3H 4R2, Canada.
***Corresponding author. Email: nfzheng@xmu.edu.cn (N.Z.);**

Ultraviolet (UV) light–induced formation of ethylene glycolate (EG) radicals on TiO_2 nanosheets was shown to be critical for preparing Pd_1/TiO_2. With abundant Pd-O interfaces, Pd_1/TiO_2 activates H_2 in a heterolytic pathway distinct from the homolytic pathway on conventional Pd heterogeneous catalysts. The Pd_1/TiO_2 catalyst exhibits extremely high catalytic activities and stabilities in hydrogenation of C=C and C=O. A turnover frequency (TOF) greater than that of surface Pd atoms on commercial Pd catalysts by a factor of >55 was demonstrated on Pd_1/TiO_2 in the hydrogenation of aldehyde at room temperature, and no decay in the catalytic activity was observed during catalysis.

Two-atom-thick TiO_2(B) nanosheets [figs. S1 to S4 (*29*)] were prepared by reacting $TiCl_4$ with EG and were used as the support (*30*). H_2PdCl_4 was introduced into a water dispersion of TiO_2(B) to allow the adsorption of Pd species (figs. S5 and S6). The mixture was then irradiated by low-density UV provided by a Xe lamp (fig. S7). After 10 min of irradiation, the Pd_1/TiO_2 catalyst was collected and washed thoroughly with water. No formation of Pd nanoparticles (NPs) was observed in transmission electron microscopy (TEM) images (Fig. 1A and fig. S8) or in the x-ray diffraction pattern (fig. S9) of the obtained Pd_1/TiO_2 catalyst, even with the loading content of Pd as high as 1.5 weight percent (wt %) as analyzed by inductively coupled plasma mass spectrometry (ICP-MS). Energy-dispersive x-ray spectroscopy (EDS) analysis in a scanning transmission electron microscope (STEM) revealed that atomic Pd was evenly dispersed in Pd_1/TiO_2 (Fig. 1B), unlike in supported Pd NPs prepared by a conventional impregnation method followed by calcination in air at 350°C (fig. S10). To verify that Pd atoms were dispersed in Pd_1/TiO_2, we performed x-ray absorption near-edge structure (XANES) and extended x-ray absorption fine structure (EXAFS) spectrometry (Fig. 1C and figs. S11 and S12). There was only one notable peak in the region 1 to 2 Å from the Pd-O contribution, and no peak in the region 2 to 3 Å from the Pd-Pd contribution, confirming the sole presence of dispersed Pd atoms in Pd_1/TiO_2 (table S1). The calcination of the as-prepared Pd_1/TiO_2 in air at 350°C removed the organic residues on the surface of Pd_1/TiO_2 and thus allowed direct observation of the atomic dispersion of Pd by aberration-corrected STEM (Fig. 1D and fig. S13).

After calcination, there were still a large number of dispersed Pd atoms on the TiO_2 support, even with the Pd loading up to 1.5 wt%. We also investigated the CO adsorption behavior of Pd_1/TiO_2 (fig. S14) to confirm the atomic dispersion of Pd on the catalyst. There was only a weak band at 2100 cm^{-1} ascribed to CO adsorbed on $Pd^{\delta+}$ in a top configuration (*31*). No signals attributed to CO adsorbed on bridge or hollow sites were observed, quite unlike supported Pd nanoparticulate catalysts (fig. S15).

Styrene hydrogenation was chosen as a model reaction to evaluate the catalytic activity of Pd_1/TiO_2. The Pd_1/TiO_2 catalyst displayed an extremely high activity and stability (Fig. 2, A and B) relative to commercial Pd/C (fig. S16), TiO_2(B)-supported Pd NPs (fig. S17), and unsupported homogeneous H_2PdCl_4 catalysts. We achieved 100% styrene conversion in 1 hour at a molar ratio of $1:10^4$ (Pd:styrene). The calculated TOF value of Pd_1/TiO_2, 8973 $hours^{-1}$, was greater than that of surface Pd atoms on the Pd/C catalyst (972 $hours^{-1}$) by a factor of 9. The reaction rate of Pd_1/TiO_2 was maintained even after 20 cycles with the same catalyst (fig. S18), which suggests that the atomically dispersed structure of Pd_1/TiO_2 was robust under the catalytic conditions. There was no detectable change in the EXAFS fitting profiles after 20 catalytic cycles (fig. S19 and table S2). In contrast, an obvious decreased activity was observed on unsupported H_2PdCl_4 in the second cycle and even at the end of the first run (fig. S20). Because styrene hydrogenation is a zero-order reaction whose reaction rate is independent of the styrene's concentration (*32*, *33*), the decline in the reaction rate of H_2PdCl_4 (Fig. 2B) was caused by the changing status of the catalyst. After reaction, small Pd NPs were detected in the reaction mixture (figs. S21 and S22).

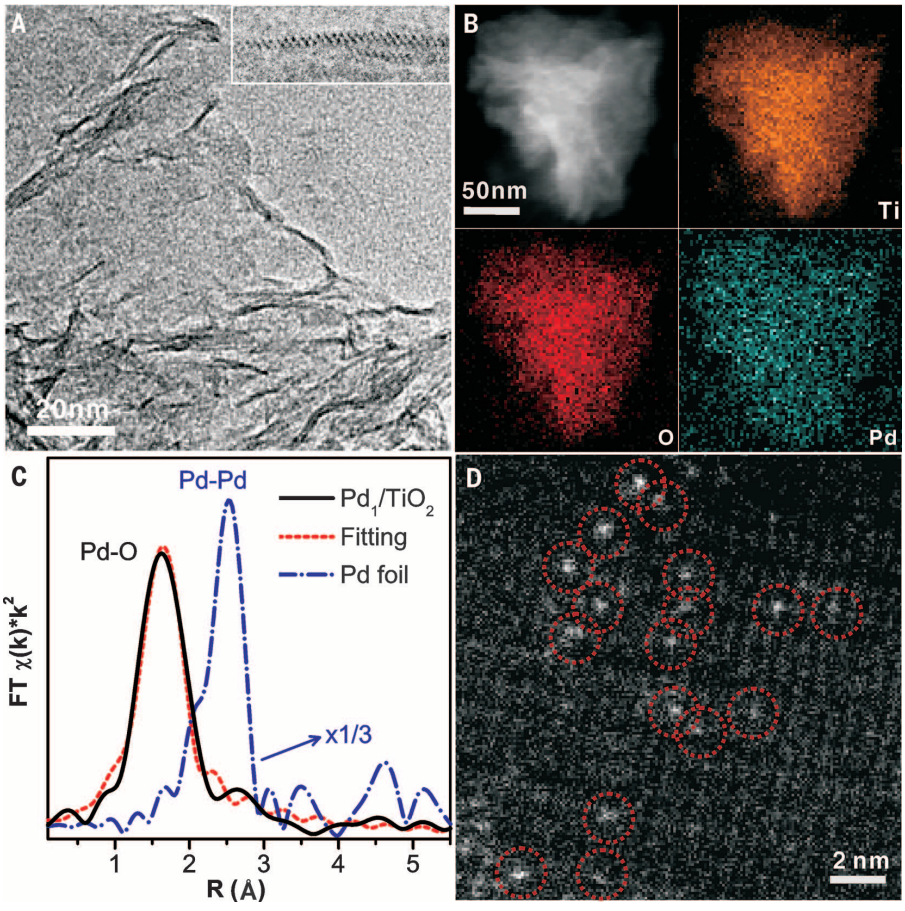

Fig. 1. Structural characterizations of Pd_1/TiO_2. (**A**) Representative TEM image of Pd_1/TiO_2. The inset is an aberration-corrected STEM image for cross sections of ultrathin TiO_2(B), showing that it is composed of only two layers of Ti atoms. (**B**) STEM-EDS elemental mapping of a single Pd_1/TiO_2 nanosheet. (**C**) FT-EXAFS spectra of Pd_1/TiO_2 and bulk palladium foil at the Pd K-edge, showing the surrounding atoms adjacent to Pd atoms. (**D**) High-resolution high-angle annular dark-field (HAADF) STEM image of Pd_1/TiO_2. The sample was calcined in air at 350°C for better contrast.

To better understand why the Pd_1/TiO_2 catalyst possessed such a high catalytic activity and stability, we prepared a catalyst (denoted $PdCl_2/TiO_2$) by the same method as for Pd_1/TiO_2 but without the UV treatment (fig. S23). No Pd-Pd bonds in $PdCl_2/TiO_2$ were detected by EXAFS (Fig. 2C and fig. S24), similar to Pd_1/TiO_2. The coordination numbers of Pd-O and Pd-Cl in the obtained $PdCl_2/TiO_2$ were 2.2 and 1.7, respectively (table S3). The Pd:Cl molar ratio of ~1:2 in the catalyst was confirmed by the elemental analysis (fig. S25). All of these data indicated that Pd atoms in $PdCl_2/TiO_2$ were in the form of individual $PdCl_2$ species bound on TiO_2(B). The presence of two Cl^- ligands on each Pd atom made the catalytic performance of $PdCl_2/TiO_2$ much poorer than that of Pd_1/TiO_2 (Fig. 2D). The reaction rate already declined during the first run and kept decreasing after every recycle, suggesting a deleterious effect of Pd-Cl bonds on the catalysis. Similar to H_2PdCl_4, the decreased activity of $PdCl_2/TiO_2$ was attributed to the sintering of Pd atoms into NPs during catalysis. EXAFS studies revealed that a peak in the region 2 to 3 Å from the Pd-Pd contribution emerged for the $PdCl_2/TiO_2$ catalyst after catalysis (Fig. 2C and table S4).

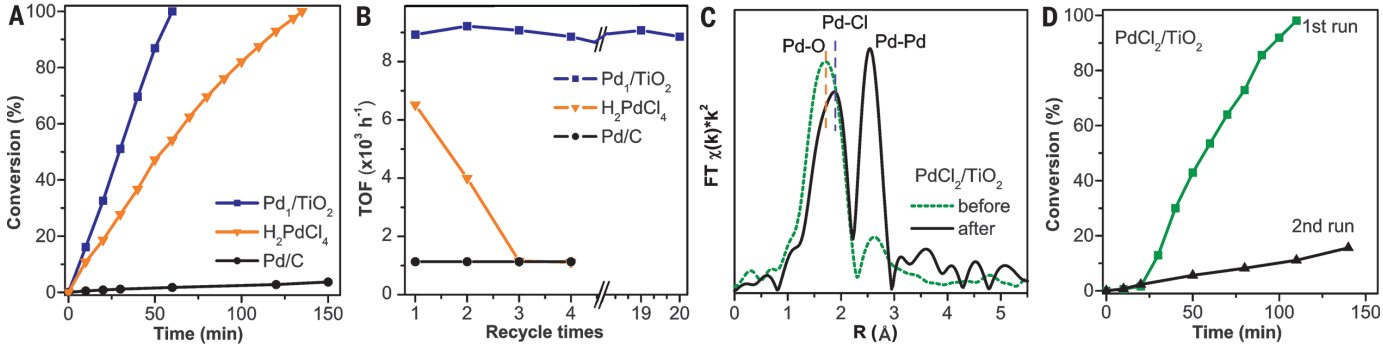

Fig. 2. Catalytic performances of Pd_1/TiO_2 and reference materials in styrene hydrogenation. (**A** and **B**) Catalytic performances for the first run (A) and TOF (B) of several recycles of repeated reactions for Pd_1/TiO_2, H_2PdCl_4, and commercial Pd/C. The same portion of Pd_1/TiO_2 catalyst was recycled and used for 20 runs without loss of activity. (**C**) FT-EXAFS spectra at the Pd K-edge of $PdCl_2/TiO_2$ before and after catalysis reaction. (**D**) First- and second-run catalytic performances of $PdCl_2/TiO_2$. Reaction conditions: ethanol, 10 ml; Pd, 0.005 μmol; styrene, 50 μmol; T = 303 K; pressure = 0.1 MPa.

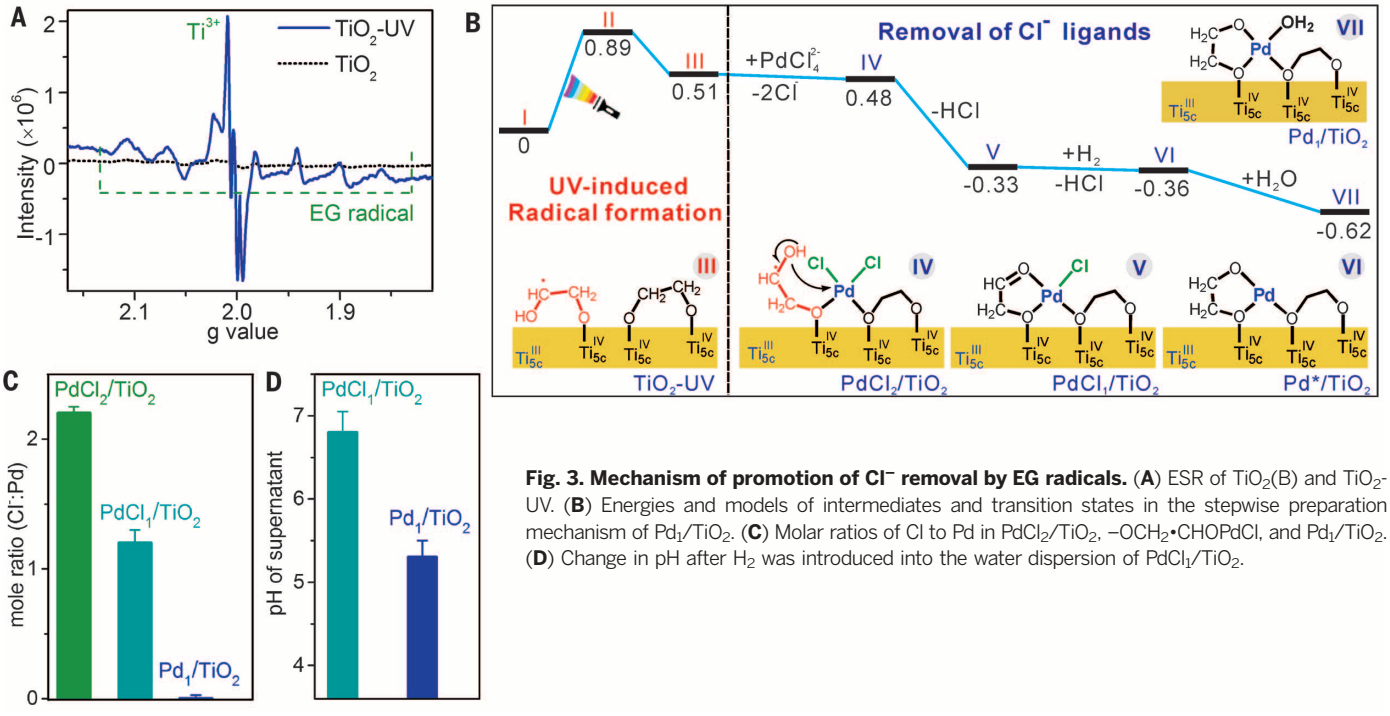

Fig. 3. Mechanism of promotion of Cl^- removal by EG radicals. (**A**) ESR of TiO_2(B) and TiO_2-UV. (**B**) Energies and models of intermediates and transition states in the stepwise preparation mechanism of Pd_1/TiO_2. (**C**) Molar ratios of Cl to Pd in $PdCl_2/TiO_2$, $-OCH_2$•CHOPdCl, and Pd_1/TiO_2. (**D**) Change in pH after H_2 was introduced into the water dispersion of $PdCl_1/TiO_2$.

Pd NPs were observed in TEM images for the used $PdCl_2/TiO_2$ catalyst (fig. S26), indicating that the presence of Pd-Cl bonds would destabilize atomically dispersed Pd on TiO_2 and induce their sintering into NP during catalysis.

The removal of Cl^- ligands on Pd under mild UV conditions appears vital for preparing highly stable and active Pd catalysts. To confirm this, we thoroughly washed $PdCl_2/TiO_2$ with water until no Cl^- was detected in the supernatant. The water dispersion of $PdCl_2/TiO_2$ was then exposed to UV for 10 min. As expected, all Cl^- ligands on $PdCl_2/TiO_2$ were released into the supernatant (figs. S25 and S27). The molar ratio of the released Cl^- to the anchored Pd was measured to be ~2, confirming the formation of the Cl^--free Pd_1/TiO_2 catalyst after the UV treatment.

The UV-induced elimination of Cl^- from $PdCl_2/TiO_2$ was attributed to the photoreactivity of TiO_2(B) nanosheets. As shown in Fig. 3A, TiO_2(B) nanosheets treated by UV alone (denoted as TiO_2-UV) already displayed an electron spin resonance (ESR) spectrum with an intense peak corresponding to a Ti^{3+} species and a set of six peaks that matched perfectly with EG radicals ($HOCH_2$•CHOH) (*34*). Similar signals were observed for the as-prepared Pd_1/TiO_2 catalyst (fig. S28). However, no obvious ESR peaks were found on the original TiO_2(B) nanosheets without UV treatment (Fig. 3A).

Together with selected-area electron diffraction (SAED) (fig. S1) and the aberration-corrected STEM (fig. S2), thermogravimetric analysis (fig. S29) and infrared (IR) spectroscopy (fig. S30) suggested that two-atom-thick TiO_2 nanosheets used in this work had TiO_2(B)(010) as their major exposed facets, and these exposed facets were highly covered by deprotonated EG (~19 wt %) (fig. S31). Once exposed to UV, electron-hole pairs were generated on TiO_2(B) nanosheets. Electrons were trapped in Ti-3d orbitals to form Ti^{3+} sites (*35*), and holes broke Ti-O bonds between glycolate and TiO_2, leading to the formation of $-OCH_2CH_2O$• radicals (from I to II in Fig. 3B) (figs. S32 and S33). Because of the presence of α-H, $-OCH_2CH_2O$• was not stable and would thus undergo hydrogen transfer to give $-OCH_2$•CHOH. According to density functional theory (DFT) calculations, such a process (from II to III in Fig. 3B) was predicted to be exothermic by 0.38 eV. Such UV-generated surface organic radicals are not unusual, as the oxidation potentials of most organic compounds lie below that of the holes in the valence band of TiO_2 (*36*–*38*). The ESR signals from the samples after washing and drying processes suggest that, once formed upon UV irradiation, the EG radicals on the surface of TiO_2 nanosheets were quite stable.

To understand how EG radicals promoted the release of Cl^- from Pd sites, we also designed a

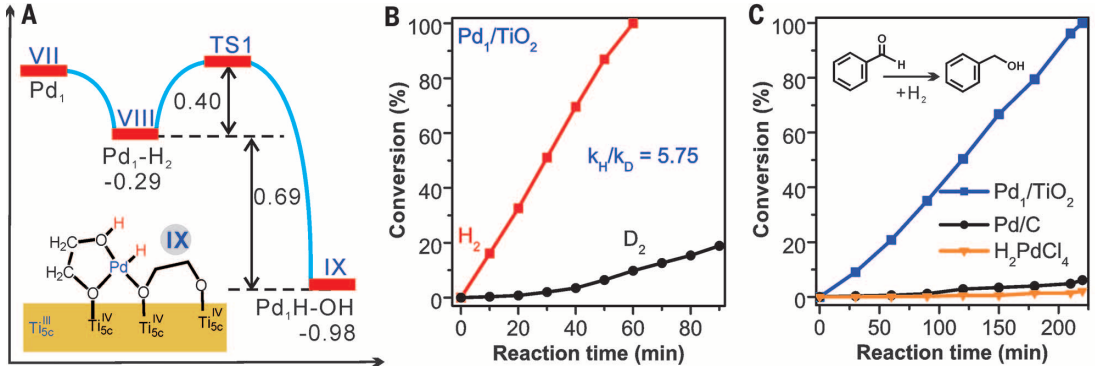

Fig. 4. Catalytic mechanism of Pd_1/TiO_2 in hydrogenation reactions. (**A**) Energies and model of intermediates and transition states in the heterolytic H_2 activation process for Pd_1/TiO_2. (**B**) Primary isotope effect observed for Pd_1/TiO_2 in styrene hydrogenation. (**C**) First-run reaction performances for Pd_1/TiO_2, Pd/C, and H_2PdCl_4 in benzaldehyde hydrogenation.

stepwise route (fig. S34) to prepare the Pd_1/TiO_2 catalyst. UV treatment was first used to obtain TiO_2-UV nanosheets containing EG radicals on their surfaces. H_2PdCl_4 was then introduced into the water dispersion of TiO_2-UV. Our calculations showed that once adsorbed onto TiO_2, each $PdCl_4^{2-}$ liberated two Cl^- ligands, yielding an intermediate with individual $PdCl_2$ units adsorbed on TiO_2 (IV in Fig. 3B) (fig. S35). Such a process was predicted to be slightly exothermic by 0.03 eV. Subsequently, the OH group in $-OCH_2$•CHOH attacked its nearby Pd site by replacing one Cl^-, leading to the formation of $PdCl_1/TiO_2$ intermediate (V in Fig. 3B) with an exothermicity of 0.81 eV. As shown in fig. S35, $PdCl_1/TiO_2$ has three Ti-O bonds and one Pd-Cl bond. Experimentally, both EXAFS data and elemental analysis showed a Cl:Pd molar ratio of ~1:1 for $PdCl_1/TiO_2$ (Fig. 3C, figs. S36 and S37, and table S4), lower than the 2:1 molar ratio in $PdCl_2/TiO_2$ made from untreated TiO_2. Moreover, mixing TiO_2(B)-UV with H_2PdCl_4 solution decreased the amount of EG radicals, as evidenced by the reduced intensity of each ESR peak (fig. S38).

All of these results strongly confirmed that the UV-generated EG radicals facilitated the removal of Cl^- on Pd and stabilized individual Pd atoms by forming more Pd-O bonds. The remaining Cl^- on $PdCl_1/TiO_2$ could be easily removed by using H_2 treatment, giving rise to H^+ and Cl^- (from V to VII in Fig. 3B) (table S5). This result explained why treating the water dispersion of $PdCl_1/TiO_2$ resulted in a pH drop from 6.8 to 5.3 (Fig. 3D). Alternatively, further UV treatment completely removed Cl^- from $PdCl_1/TiO_2$ (fig. S39), also leading to the formation of Pd_1/TiO_2. The catalyst prepared in the stepwise procedure showed the same catalytic properties as that prepared by the one-pot method in which the aqueous mixture of TiO_2 and H_2PdCl_4 was directly treated with UV (fig. S40). More important, the insight into the formation mechanism of Pd_1/TiO_2 allowed us to prepare the catalyst in large scale by using a continuous UV-flow reactor (fig. S41).

To evaluate the importance of EG radicals in the preparation of the atomically dispersed Pd_1/TiO_2 catalyst, we also synthesized EG-free TiO_2 by calcination of TiO_2(B) nanosheets at 350°C in air and used it as the support for the catalyst preparation. A photochemical strategy similar to that used in the one-step preparation of Pd_1/TiO_2 was applied to load Pd onto EG-free TiO_2, but Pd NPs were formed (fig. S42); this result shows that surface EG helps to stabilize atomically dispersed Pd catalysts during their preparation. When surface EG was removed by calcination, the obtained Pd_1/TiO_2-cal catalyst displayed a substantially decreased activity with a TOF of only 1930 $hours^{-1}$ (fig. S43).

It is generally accepted that H_2 would undergo homolytic dissociation on conventional Pd particulate catalysts into H atoms with partially negative charge ($H^{\delta-}$) (*39*). In this case, the presence of more than two Pd atoms in the vicinity is required. However, all Pd atoms in Pd_1/TiO_2 are individually dispersed, with no Pd-Pd pairs available for homolytic dissociation of H_2, so the dissociation of H_2 must go via an alternative pathway on Pd_1/TiO_2. According to our DFT calculations (Fig. 4A and figs. S44 to S46), H_2 adsorbed on Pd was readily split into two H atoms. One of the H atoms moved to a nearby oxygen on EG to yield O-$H^{\delta+}$, leaving the other H atom on Pd as $H^{\delta-}$ (Fig. 4A). This step was calculated to be exothermic by 0.69 eV and exhibited a barrier of 0.40 eV. We expected that both Pd-$H^{\delta-}$ and O-$H^{\delta+}$ should then be involved in the hydrogenation catalysis. DFT calculations revealed that the hydrogenation of styrene using Pd_1/TiO_2 followed a stepwise process. Computationally, we considered two possible pathways (figs. S44 to S46), one beginning with $H^{\delta-}$ transfer from Pd to C=C and the other beginning with $H^{\delta+}$ transfer. The first of these is energetically favorable, with a barrier of only 0.47 eV required for the $H^{\delta-}$ transfer from Pd to the terminal CH_2 to make the half-hydrogenated intermediate, which in turn adds $H^{\delta+}$ from a nearby O-H group by overcoming a barrier of 0.73 eV. This pathway leads to the formation of ethylbenzene and simultaneously recovers the Pd-EG interfaces.

To test the proposed mechanism, we explored the kinetic isotope effect (KIE) with the use of D_2 in styrene hydrogenation. For Pd/C, the reaction was slowed down by a factor of 1.43 (fig. S47) as a result of the zero-point energy difference between isotopic isomers. However, on Pd_1/TiO_2, a larger KIE was observed (ratio of reaction rates using H_2 and D_2, k_H/k_D = 5.75) (Fig. 4B) because the bond cleavage was O-D rather than Pd-D in the rate-determining step. Both our IR spectroscopy and nuclear magnetic resonance measurements, which were performed with deuterium-labeled reagents, confirmed the proposed mechanism (figs. S48 and S49). Such a large KIE in hydrogenation caused by the participation of both $H^{\delta-}$ and $H^{\delta+}$ has usually been observed on homogeneous catalysts (e.g., Au, Pd, and Ru complexes) (*7*, *40*, *41*) but has not been reported on heterogeneous Pd catalysts. In this regard, atomically dispersed metal catalysts can share the same hydrogenation mechanism as homogeneous catalysts.

Because the heterolytic activation of H_2 yielded both $H^{\delta-}$ and $H^{\delta+}$ at the Pd-O interface, Pd_1/TiO_2 should allow better hydrogenation of polar unsaturated bonds. As expected, in the hydrogenation of benzaldehyde, we observed a much superior catalytic performance by Pd_1/TiO_2 (Fig. 4C and fig. S50). Pd_1/TiO_2 readily converted all of the benzaldehyde into benzyl alcohol in 3.5 hours at room temperature with a TOF of 1002 $hours^{-1}$. No decay in the catalysis was observed after the catalyst was used for five cycles. In comparison, both Pd/C and H_2PdCl_4 showed negligible activity under the same catalytic condition, with TOF less than 18 $hours^{-1}$. This work demonstrates that upgrading catalytically active components from nanoparticles to single atoms not only boosts the catalytic reaction because of the high atom efficiency, but also endows atomically dispersed catalysts with catalytic capability that conventional nanocatalysts do not possess.

REFERENCES AND NOTES

1. B. Qiao *et al.*, *Nat. Chem.* **3**, 634–641 (2011).
2. K. Ding *et al.*, *Science* **350**, 189–192 (2015).
3. J. H. Kwak *et al.*, *Science* **325**, 1670–1673 (2009).
4. Y. Zhai *et al.*, *Science* **329**, 1633–1636 (2010).
5. Q. Fu, H. Saltsburg, M. Flytzani-Stephanopoulos, *Science* **301**, 935–938 (2003).
6. M. Yang *et al.*, *Science* **346**, 1498–1501 (2014).
7. A. Comas-Vives *et al.*, *J. Am. Chem. Soc.* **128**, 4756–4765 (2006).
8. X. Zhang, H. Shi, B. Q. Xu, *Angew. Chem. Int. Ed.* **44**, 7132–7135 (2005).
9. G. Vilé *et al.*, *Angew. Chem. Int. Ed.* **54**, 11265–11269 (2015).
10. S. Abbet *et al.*, *J. Am. Chem. Soc.* **122**, 3453–3457 (2000).
11. H. Yan *et al.*, *J. Am. Chem. Soc.* **137**, 10484–10487 (2015).
12. E. J. Peterson *et al.*, *Nat. Commun.* **5**, 4885 (2014).
13. J. Lin *et al.*, *J. Am. Chem. Soc.* **135**, 15314–15317 (2013).

14. V. Ortalan, A. Uzun, B. C. Gates, N. D. Browning, *Nat. Nanotechnol.* **5**, 506–510 (2010).
15. J. M. Thomas, *Nature* **525**, 325–326 (2015).
16. W. E. Kaden, T. Wu, W. A. Kunkel, S. L. Anderson, *Science* **326**, 826–829 (2009).
17. J. M. Thomas, Z. Saghi, P. L. Gai, *Top. Catal.* **54**, 588–594 (2011).
18. G. Kyriakou *et al.*, *Science* **335**, 1209–1212 (2012).
19. M. Yang, L. F. Allard, M. Flytzani-Stephanopoulos, *J. Am. Chem. Soc.* **135**, 3768–3771 (2013).
20. H. Wei *et al.*, *Nat. Commun.* **5**, 5634 (2014).
21. M. Yang *et al.*, *J. Am. Chem. Soc.* **137**, 3470–3473 (2015).
22. S. Sun *et al.*, *Sci. Rep.* **3**, 1775 (2013).
23. J. O. Ehresmann *et al.*, *Angew. Chem. Int. Ed.* **45**, 574–576 (2006).
24. A. Uzun, B. C. Gates, *J. Am. Chem. Soc.* **131**, 15887–15894 (2009).
25. X.-Q. Gong, A. Selloni, O. Dulub, P. Jacobson, U. Diebold, *J. Am. Chem. Soc.* **130**, 370–381 (2008).
26. D. Matthey *et al.*, *Science* **315**, 1692–1696 (2007).
27. M. Flytzani-Stephanopoulos, B. C. Gates, *Annu. Rev. Chem. Biomol. Eng.* **3**, 545–574 (2012).
28. J. M. Thomas, R. Raja, *Top. Catal.* **40**, 3–17 (2006).
29. See supplementary materials on *Science* Online.
30. G. Xiang, T. Li, J. Zhuang, X. Wang, *Chem. Commun. (Camb.)* **46**, 6801–6803 (2010).
31. V. V. Kaichev *et al.*, *J. Phys. Chem. B* **107**, 3522–3527 (2003).
32. Z. Király, B. Veisz, Á. Mastalir, *Catal. Lett.* **95**, 57–59 (2004).
33. B. Veisz, Z. Király, L. Tóth, B. Pécz, *Chem. Mater.* **14**, 2882–2888 (2002).
34. T. Shiga, *J. Phys. Chem.* **69**, 3805–3814 (1965).
35. R. F. Howe, M. Gratzel, *J. Phys. Chem.* **89**, 4495–4499 (1985).
36. M. R. Hoffmann, S. T. Martin, W. Choi, D. W. Bahnemann, *Chem. Rev.* **95**, 69–96 (1995).
37. Y. Chen, S. Yang, K. Wang, L. Lou, *J. Photochem. Photobiol. Chem.* **172**, 47–54 (2005).
38. L. Yu *et al.*, *Phys. Chem. Chem. Phys.* **14**, 3589–3595 (2012).
39. S. Syrenova *et al.*, *Nat. Mater.* **14**, 1236–1244 (2015).
40. A. M. Kluwer, T. S. Koblenz, T. Jonischkeit, K. Woelk, C. J. Elsevier, *J. Am. Chem. Soc.* **127**, 15470–15480 (2005).
41. A. Dedieu, S. Humbel, C. Elsevier, C. Grauffel, *Theor. Chem. Acc.* **112**, 305–312 (2004).

ACKNOWLEDGMENTS

Supported by Ministry of Science and Technology of China grant 2015CB932303; National Natural Science Foundation of China grants 21420102001, 21131005, 21390390, 21133004, 21373167, 21573178, and 21333008; a NSERC CGS Alexander Graham Bell scholarship (D.M.C.); and a NSERC Discovery grant (P.Z.). We thank the XAFS station (BL14W1) of the Shanghai Synchrotron Radiation Facility.

SUPPLEMENTARY MATERIALS

www.sciencemag.org/content/352/6287/797/suppl/DC1
Materials and Methods
Supplementary Text
Figs. S1 to S50
Tables S1 to S5
References (*42*–*55*)

22 February 2016; accepted 5 April 2016
10.1126/science.aaf5251

ORGANIC CHEMISTRY

A general alkyl-alkyl cross-coupling enabled by redox-active esters and alkylzinc reagents

Tian Qin,[1]* Josep Cornella,[1]* Chao Li,[1]* Lara R. Malins,[1] Jacob T. Edwards,[1] Shuhei Kawamura,[1] Brad D. Maxwell,[2] Martin D. Eastgate,[3] Phil S. Baran[1]†

Alkyl carboxylic acids are ubiquitous in all facets of chemical science, from natural products to polymers, and represent an ideal starting material with which to forge new connections. This study demonstrates how the same activating principles used for decades to make simple C–N (amide) bonds from carboxylic acids with loss of water can be used to make C–C bonds through coupling with dialkylzinc reagents and loss of carbon dioxide. This disconnection strategy benefits from the use of a simple, inexpensive nickel catalyst and exhibits a remarkably broad scope across a range of substrates (>70 examples).

The heart of chemical synthesis relies on forging new C–C bonds, with the evolution and advancement of the field being easily correlated to new developments on this front. For example, pioneering work on the cross-coupling of halogenated aromatic or vinylic (sp^2) systems (Heck, Suzuki, Negishi, and Stille) has transformed the practice of organic synthesis (*1*). Similarly, a general and practical approach to $C(sp^3)$–$C(sp^3)$ variants would have the potential to open up new vistas in retrosynthetic analysis. Indeed, such transformations have been on organic chemists' wish list for well over a century (*2*, *3*). Historically, alkyl-alkyl transition metal–catalyzed cross-coupling reactions have been difficult to accomplish, but examples can be traced to the early work of Kharasch in the 1950s (*4*), followed by Noller (*5*, *6*) and Kochi and Tamura (*7*, *8*) in the 1960s to more recent work from the groups of Suzuki (*9*), Fu (*10*), Knochel (*11*), Kambe (*12*), Oshima (*13*), and many others (*14*). Thus far, the vast majority of approaches to this problem have involved the coupling of alkyl halides (or related species) to organometallic reagents (*15*–*18*). However, the limited availability, perceived instability, and frequent toxicity of alkyl halides has perhaps prevented the area of alkyl cross-coupling from blossoming. If one only considers convenience, stability, and availability as desired attributes in a functional group for such a coupling, the carboxylic acid reigns supreme (Fig. 1A). Alkyl carboxylic acids are ubiquitous in every aspect of chemistry and can be readily found in medicines, materials, and natural products and in the pages of commercial chemical supplier catalogs. They are a stable functional group, nontoxic, and eminently diversifiable owing to the field of combinatorial chemistry, in which they are the "workhorse" building block. Although certain carboxylic acids have already been demonstrated to engage in cross-coupling reactions (*19*), the use of alkyl carboxylic acids in alkyl-alkyl cross-coupling remains elusive.

Carboxylic acids can be primed for reaction through a process known as activation (such as formation of an active ester, –OA*), dating back to the classic work of Sheehan in the synthesis of penicillin (*20*). Once activated, a gateway opens to access a myriad of related functional groups such as amides, ketones, esters, or alcohols via addition of a nucleophile or alternative oxidation states by the formal addition of hydrogen. In this Report, we present a broadly useful transform that is able to forge $C(sp^3)$–$C(sp^3)$ bonds via this age-old activation process.

We recently reported a Ni-catalyzed decarboxylative cross-coupling of alkyl carboxylic acids with arylzinc reagents to forge $C(sp^3)$–$C(sp^2)$ bonds by repurposing activating methods more typically associated with amide-bond formation (*21*, *22*). Certain active esters [such as HOAt (*N*-hydroxy-7-azabenzotriazole), HOBt (*N*-hydroxybenzotriazole), NHPI (*N*-hydroxyphthalimide), and TCNHPI (*N*-hydroxytetrachlorophthalimide)] can accept an electron to trigger an ensuing cascade of events that liberates CO_2 from the parent alkyl group (Alk_1); such esters (*23*) are termed redox-active (*21*, *22*). The application of this chemistry to sp^3–sp^3 C–C bond formation poses a number of substantial challenges, with potentially unproductive pathways far outnumbering the desired reaction (Fig. 1B) (*15*–*18*). For example, β-hydride elimination from the alkyl metal intermediates, dimerization of the organometallic reagent, reduction of the electrophile, and proto-demetallation are problems that also historically plague traditional $C(sp^3)$–$C(sp^3)$ cross-coupling reactions. With a redox-active ester as an electrophile, oxidative addition of low-valent Ni into the activated C–O bond could result in the formation of an acyl-Ni complex, which could reductively eliminate and ultimately result in undesired ketone by-products. These fundamental challenges notwithstanding, we describe a straightforward solution to this problem.

Dialkylzinc reagents were chosen for the organometallic coupling partner because of their

[1]Department of Chemistry, Scripps Research Institute, 10550 North Torrey Pines Road, La Jolla, CA 92037, USA. [2]Discovery Chemistry Platforms–Radiochemistry, Bristol-Myers Squibb, Post Office Box 4000, Princeton, NJ, USA. [3]Chemical Development, Bristol-Myers Squibb, One Squibb Drive, New Brunswick, NJ 08903, USA.
*These authors contributed equally to this work. †Corresponding author. Email: pbaran@scripps.edu

Photochemical route for synthesizing atomically dispersed palladium catalysts

Pengxin Liu, Yun Zhao, Ruixuan Qin, Shiguang Mo, Guangxu Chen, Lin Gu, Daniel M. Chevrier, Peng Zhang, Qing Guo, Dandan Zang, Binghui Wu, Gang Fu and Nanfeng Zheng (May 12, 2016)
Science **352** (6287), 797-800. [doi: 10.1126/science.aaf5251]

Editor's Summary

Lightly dispersed palladium

Catalysts made from atomically dispersed metal atoms on oxide supports can exhibit very high per atom activity. However, the low loadings needed to prevent metal particle formation can limit overall performance. Liu *et al.* stably decorated titanium oxide nanosheets with relatively high loadings of single palladium atoms by reducing the ions with ultraviolet light and ethylene glycol. These catalysts cleaved H_2 into atoms and were highly effective for hydrogenating alkenes and aldehydes.

Science, this issue p. 797

Science (print ISSN 0036-8075; online ISSN 1095-9203) is published weekly, except the last week in December, by the American Association for the Advancement of Science, 1200 New York Avenue NW, Washington, DC 20005.